Scientific and Social Research, 2026, Volume 8, Issue 5
http://ojs.bbwpublisher.com/index.php/ssr
Online ISSN: 2981-9946
Print ISSN: 2661-4332

Enrichment and Detection Technology of Wheat Stem Rust Spores Based on Microfluidic Chips

Wenbo Sun[1], Hao Li[1], Ping'an Ma[1], Shan Wei[1], Yuansen Hu[1], Yujie Lu[2], Shuaibing Zhang[1]*

[1]School of Biological Engineering, Henan University of Technology, Zhengzhou 450001, China
[2]School of Food Science and Technology, Jiangsu University of Science and Technology, Zhenjiang 212002, China

**Author to whom correspondence should be addressed.*

Abstract: To address the problems of low spore capture efficiency and insufficient automation in wheat stem rust monitoring, this study developed an integrated spore detection system featuring automatic capture, identification, and remote monitoring. A microfluidic chip with a four-stage micro-separation structure was designed and optimized via numerical simulation and fabricated using soft lithography with PDMS. An aerosol generator was used to simulate spore diffusion, a microscopic imaging system was applied to obtain spore morphological features, and an intelligent spore recognition model was established based on the YOLOv8 algorithm. Finally, a spore capture and analyzer integrated with environmental monitoring and remote communication functions was developed. The results showed that the simulated enrichment efficiencies of the microfluidic chip for spores of 100 μm, 50 μm, 25 μm, and 10 μm were 89.3%, 92.6%, 95.1%, and 90.8%, respectively, with an actual enrichment efficiency of 86.67%. The mAP@50 of the spore recognition model reached 96.7%, with precision and recall of 93.8% and 89.5%, respectively. The system established in this study enables high-efficiency capture, accurate identification, and full-process unattended operation of *Puccinia graminis* f. sp. *tritici* spores, providing technical support for the intelligent monitoring of airborne crop diseases.

Key words: Wheat stem rust; Ug99; Spore capture; Microfluidics; Spore detection

Online publication: June 5, 2026

1. Introduction

Wheat stem rust, caused by *Puccinia graminis* f. sp. *tritici* (Pgt), is a devastating airborne disease that poses a persistent threat to the safe production of wheat worldwide [1–3]. As an obligate parasitic fungus, Pgt mainly infects wheat stems and leaf sheaths, forming reddish-brown to tan, elliptical or elongated uredinium on diseased tissues. After rupturing the host epidermis, mature uredinia release large numbers of urediniospores that spread long distances via air currents, leading to rapid disease spread. In severe cases, the pathogen can infect wheat spikes, causing poor spike development and shriveled grains, resulting in significant reductions in wheat yield and quality [4–5].

Current integrated management strategies for wheat stem rust mainly rely on breeding resistant varieties, agricultural measures (e.g., crop rotation), and chemical control, among which disease monitoring provides critical support for early warning and decision-making [6–7]. Wheat varieties carrying the *Sr31* resistance gene (derived from the 1BL/1RS translocation line) can effectively control this disease. However, since the emergence of Ug99 and its derivative races, which can overcome resistance mediated by the *Sr31* gene and have spread to major wheat-producing areas, previously resistant varieties have lost their protective effects [8]. This evolution highlights the urgency of developing new monitoring technologies and prevention systems. In integrated management, the core of disease monitoring lies in the dynamic capture and quantitative analysis of airborne urediniospores to provide early signals for epidemic prediction. Nevertheless, existing spore capture technologies generally suffer from low efficiency and insufficient automation, making it difficult to achieve efficient and accurate monitoring of pathogenic spores, thereby limiting the effective construction of early warning systems for wheat stem rust. Therefore, developing an efficient monitoring technology capable of automatic capture, accurate identification, and intelligent analysis of spores is of great theoretical and practical significance for improving the prevention and control of wheat stem rust.

At present, monitoring of wheat stem rust (Pgt) mainly relies on field visual inspection and passive spore capture techniques. These traditional methods have obvious limitations in sensitivity, accuracy, and timeliness, especially failing to effectively capture low-density urediniospore populations critical for early warning. Although molecular diagnostic techniques (e.g., PCR and next-generation sequencing, NGS) can significantly improve detection sensitivity and specificity, their high costs, reliance on professional equipment, and complex operating procedures restrict their popularization in large-scale field monitoring [9]. In recent years, microfluidic chip technology has provided a new approach for airborne microbial research due to its advantages in high-throughput and automated microbial detection. Through precisely designed microchannel structures and control strategies, this technology can integrate functional units such as sampling, separation, and enrichment to achieve efficient capture and identification of target microorganisms based on physical or biochemical characteristics [10]. However, the systematic application of microfluidic technology to the specific detection of airborne wheat stem rust spores has not been reported to date.

To overcome the above technical bottlenecks, this study developed an airborne Pgt urediniospore enrichment and detection system based on the integration of microfluidics and microscopic imaging. The core of the system includes a microfluidic chip separation and enrichment module, a microscopic imaging module, an environmental sensing module, and a cloud data processing module. Specifically, after being captured and enriched by the microfluidic chip, spores are automatically imaged by the integrated microscopic system. Image data are transmitted to the cloud platform via 4G networks for feature extraction and intelligent identification, finally realizing automatic counting and species identification of spores. The system can not only record environmental parameters such as temperature and humidity in real time but also provide a feasible technical solution for establishing an early risk warning system for wheat stem rust.

2. Materials and methods

2.1. Materials and instruments

Urediniospores of *Puccinia graminis* f. sp. *tritici* were provided by Shenyang Agricultural University. Microfluidic chips were fabricated by Micro & Nano Cube Technology (Beijing) Co., Ltd. A metallographic microscope was purchased from Shenzhen Haiyue Electronics Co., Ltd.

2.2. Working principle of the microfluidic chip

The movement of airborne Pgt urediniospores in microchannels belongs to sparse two-phase flow at low Reynolds numbers [11]. The Reynolds number is expressed as:

$Re = \rho v d/\eta$

where ρ, v, and η are the airflow density (kg/m³), velocity (m/s), and viscosity coefficient (Pa·s), respectively; d is the characteristic length of the airflow (m). When airflow bypasses obstacles and suddenly changes direction, it forms a curved path. With airflow variation, suspended spores move along curved streamlines. The motion characteristics of spores in microfluidic chip channels can be represented by the Stokes number (Stk):

$Stk = t_0 u_0 / L_0$

where t_0 is the spore relaxation time (s), u_0 is the flow velocity of gas passing obstacles (m/s), and L_0 is the characteristic size of obstacles (m). When $Stk > 1$, streamlines bypass obstacles while particles maintain their original direction, causing particle impaction; when $Stk \leq 1$, particles follow streamlines to deflect. When Pgt spores accelerate in gas, they drive surrounding gas to accelerate, equivalent to gaining additional mass. The added mass force (F_t) is expressed as:

$F_t = (1/12) d_p^3 \rho [d(v - v_p)/dt]$

where d_p is the spore particle size (m), ρ is the gas density (kg/m³), v is the gas velocity vector (m/s), and v_p is the spore velocity vector (m/s).

2.3. Design and numerical simulation of the microfluidic chip

The two-dimensional structure of the microfluidic chip is shown in **Figure 1**. The chip adopts a four-stage series inertial separation structure, each stage containing an inertial separation channel and a corresponding spore enrichment zone. The working principle is as follows: sample airflow containing spores enters the first-stage structure from the main inlet and is confined near the central axis of the microchannel under the focusing effect of sheath flow. As spores move with the airflow, they exhibit different inertia due to differences in size and mass: larger spores cannot follow curved streamlines and deviate from the main flow into the first enrichment zone, while spores with smaller inertia continue forward with the airflow and enter the next-stage structure through the separation channel for further sorting. The two-dimensional structure of the chip was drawn using AutoCAD 2020 software. To optimize chip performance and predict spore trajectories, the "Particle Tracing" module in COMSOL Multiphysics 6.0 software was used for numerical simulation of internal flow fields and spore motion. Simulation parameters were set as follows: 100 uniformly distributed tracer particles were released at each inlet to simulate spores; particle density was set to 1000 kg/m³; inlet flow rate was uniformly set to 15 mL/min [12].

2.4. Fabrication of the microfluidic chip

The microfluidic chip was fabricated using soft lithography based on SU-8 photolithography and polydimethylsiloxane (PDMS) replication. First, substrate pretreatment was performed: silicon wafers were immersed in a nanoscale cleaning solution for 10 minutes, rinsed with deionized water, spin-dried, and baked on a 200°C hot plate for 20 minutes to ensure complete dryness. Next, SU-8 photoresist was spin-coated and soft-baked: 80 μm-thick SU-8 photoresist was uniformly coated on silicon wafers by controlling rotation speed, pre-baked at 65°C for 3 minutes, and further baked at 95°C for 9 minutes. In the exposure stage, SU-8 photoresist was exposed to UV light through a photomask (intensity 55 mJ/cm², time 6.5 seconds), followed

by post-exposure baking: treated at 65°C for 2 minutes and 95°C for 7 minutes to complete cross-linking. Then, development and mold formation were performed: silicon wafers were immersed in SU-8 developer for 7 minutes, rinsed with isopropanol, and blow-dried with pressurized nitrogen, finally obtaining SU-8 microstructural molds with a height of 80 μm. In the soft lithography replication step, PDMS prepolymer and curing agent were mixed at a mass ratio of 10:1, stirred evenly, degassed under vacuum for 40 minutes, poured into SU-8 molds, and cured at 65°C for 4 hours. After curing, PDMS replicas were peeled off, cut, punched, and bonded with glass slides via oxygen plasma treatment (300 mTorr, 45 seconds) to form sealed PDMS microfluidic chips [13].

2.5. Spore microscopy and model construction

To observe and count wheat stem rust spores, a microscopic imaging system composed of an HY-6110 camera (12 megapixels), a metallographic microscope tube, and a 10× long-focus objective lens was constructed to collect spore images and create unique labels for each image. Training set images were manually annotated using Roboflow annotation tools, and sample diversity was expanded through data augmentation. Based on the YOLOv8 model pre-trained on large datasets, a wheat stem rust spore detection model was constructed using transfer learning; a total of 828 images were used for model training, including 346 original collected images and 482 augmented images to improve model generalization ability. To quantitatively evaluate the performance of the spore recognition model, precision (P), recall (R), and mean average precision (mAP) were used as evaluation indicators [14–15].

2.6. Development of the spore capture and analyzer

The spore capture and analyzer were developed based on modular integration, realizing automatic monitoring through multi-system collaboration. The spore capture unit adopted a miniature vacuum pump (sampling time adjustable from 1–255 minutes) to drive the microfluidic enrichment device, completing directional capture and concentration of airborne pathogenic spores. The imaging unit integrated an 8-megapixel industrial camera and a 40× optical microscopic system, cooperating with a slide limit sensor (accuracy ±0.1 mm) and a remote calibration algorithm to achieve high-definition collection and precise positioning of spore images (resolution up to 3.2 μm/pixel). The control core was equipped with an Android industrial touch screen (quad-core 1.6 GHz processor, RAM 2 GB), connecting to the sensor network through multiple interfaces (2×RS485, 1×USB 3.0, etc.) to monitor ambient temperature and humidity in real time (range -20~70°C, 0–95% RH). The communication and operation system supported 4G/Wi-Fi/Ethernet multi-mode transmission (based on TCP/HTTP protocol), with 500,000 offline data cache capacity and continuous system optimization through OTA upgrade. The whole machine was integrated into a 201 stainless steel box of 540 mm × 420 mm × 900 mm, with operating power consumption ≤20 W, standby power consumption ≤8 W, and insulation resistance ≥2.5 MΩ, finally realizing full-process automation from spore capture, microscopic imaging to cloud data transmission.

2.7. Statistical analysis

All experimental data were statistically processed using SAS 9.2 software, and data visualization and statistical charts were completed using GraphPad Prism 5.0.

3. Results and analysis

3.1. Numerical simulation results of the microfluidic chip

Based on aerodynamic principles and size characteristics of airborne particles, this study designed a microfluidic chip with a four-stage micro-separation structure for enriching airborne spores with diameters of approximately 100 μm, 50 μm, 25 μm, and 10 μm, respectively. Through structural optimization and simulation analysis of spore enrichment efficiency using COMSOL Multiphysics 6.0 software, the chip structure and size achieving the highest enrichment efficiency in each zone were finally determined (**Figure 1A, B**). Specific chip parameters are as follows: all microchannel depths were unified at 1 mm, the channel length of the initial micro-separation structure was 2 cm, inlet channel widths were all 2 mm; outlet channel widths were all 1 mm, enrichment zone radii were all 2.5 mm, and all microchannel heights were 1 mm (Figure 1C). Numerical simulation results showed that the enrichment efficiencies of the four enrichment zones in the chip for airborne particles with diameters of approximately 100 μm, 50 μm, 25 μm, and 10 μm were 89.3%, 92.6%, 95.1%, and 90.8%, respectively (**Figure 2**).

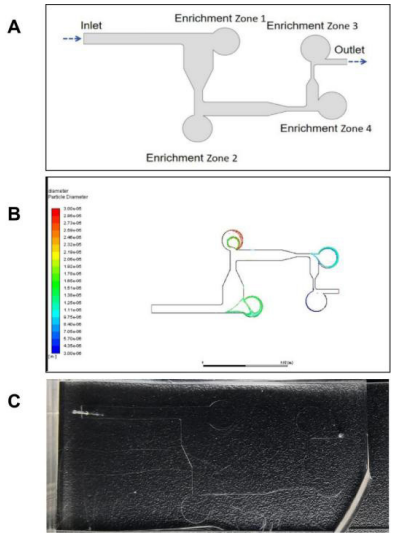

Figure 1. Microfluidic chip design (A), numerical simulation (B), and fabrication (C)

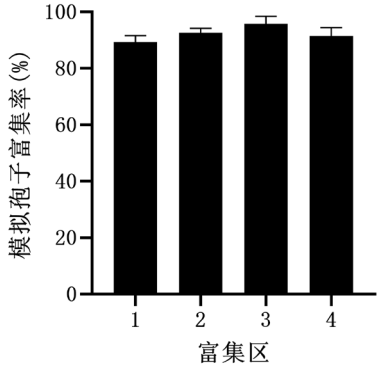

Figure 2. Enrichment efficiency of four enrichment zones in the microfluidic chip for particles with diameters of approximately 100 μm, 50 μm, 25 μm, and 10 μm in the air

3.2. Microscopic observation of Pgt urediniospores

A microscopic imaging system composed of an HY-6110 camera (12 megapixels), a metallographic microscope tube, and a 10× long-focus objective lens was constructed (**Figure 3**) for morphological observation and counting of wheat stem rust urediniospores. The resolution of images obtained by this system reached 3.2 μm/pixel, clearly presenting the fine structure on the spore surface. Observation results showed that urediniospores were typically elliptical, with an average long axis of 28–36 μm and short axis of 18–24 μm (**Figure 4**). Under the metallographic microscope, spore edges formed bright blue-white halos due to light refraction; the main body of spores was dark yellowish-brown to orange-gold, and granular cytoplasmic distribution could be seen inside. Spores had regular morphology, smooth surfaces, and a typical umbilical depression structure in the middle (**Figure 5**). These morphological characteristics were highly consistent with those of wheat stem rust urediniospores reported in the literature, laying a solid foundation for the subsequent construction of digital spore morphological models and automatic identification.

Figure 3. Microscopic photography system

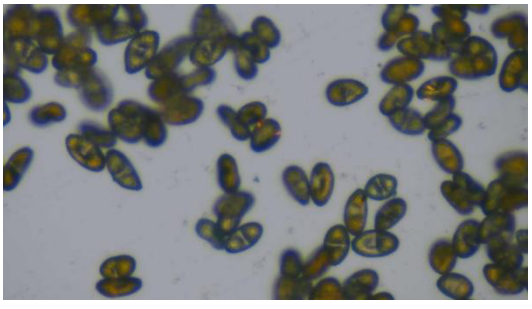

Figure 4. The morphology of wheat stem rust spores observed using the constructed microscopic photography device

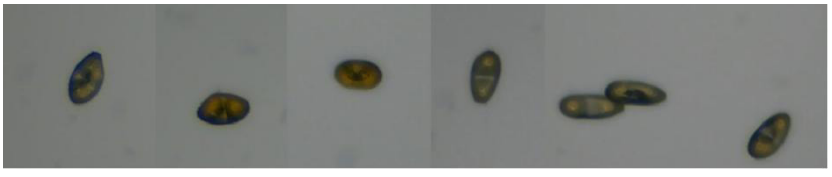

Figure 5. Morphology of wheat straw rust spores

3.3. Experimental results of spore enrichment by the microfluidic chip

Pgt urediniospore suspension was placed in an aerosol generator, and compressed air was input into the generator through an air pump to form a bioaerosol flow. After passing through a diffusion dryer to remove moisture, the aerosol flow rate was controlled at 15 mL/min via a flow meter (range 2.5–25 mL/min), consistent with chip simulation parameters. The aerosol flowed into the microfluidic chip channel to complete spore separation and enrichment, and the enrichment process was terminated after 2 minutes of air pump operation. The chip was directly observed under a microscope to count the number of Pgt urediniospores in each enrichment zone. To verify the actual enrichment efficiency of the chip, 6 repeated experiments were conducted. The number of spores in the center and edge of the four enrichment zones of each chip was counted under a microscope, the average number of spores in each enrichment zone in each experiment was calculated, and the number of spores in other channels was simultaneously counted. The actual enrichment efficiency of the microfluidic chip for Pgt urediniospores was finally determined to be 86.67% (**Figure 6**).

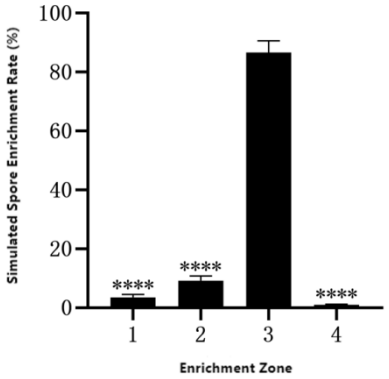

Figure 6. The actual enrichment rates of wheat stem rust spores in different enrichment zones

3.4. Construction of the Pgt urediniospore model

Wheat stem rust spore images were collected based on the previously constructed microscopic imaging system. A total of 828 training images (including 346 original images and their derived data) were manually annotated and augmented using Roboflow tools. Based on the YOLOv8 model pre-trained on the COCO dataset, a spore detection model was constructed using transfer learning. Quantitative evaluation results of the model showed excellent performance: mAP@50 reached 96.7%, precision was 93.8%, and recall was 89.5% (**Figure 7**). Qualitative evaluation showed that the system could simultaneously output visualized images with detection boxes and structured data, including bounding box coordinates and category confidence. Despite challenges such as spore overlap and fluctuating image quality, the model achieved a recognition accuracy of over 90% in practical applications, providing key technical support for the development of spore monitoring equipment integrating microfluidic chip capture, microscopic imaging, and intelligent recognition.

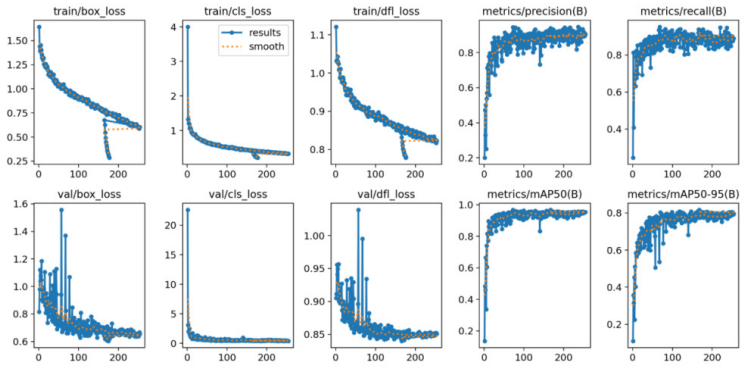

Figure 7. Training data for wheat straw rust spore model

3.5. Trial production and application of the spore capture and analyzer

Based on previous research, an automated spore capture and analyzer for wheat stem rust monitoring was successfully trial-produced (**Figure 8**). The instrument integrates five core modules: spore capture, microscopic imaging, intelligent recognition, environmental monitoring, and remote communication. Specifically, microfluidic chip technology was adopted to achieve efficient directional capture of spores; a combined imaging system of an 8-megapixel industrial camera and a 40× optical microscope completed automatic collection of high-definition images; images were automatically recognized after comparison with the spore model library via cloud AI algorithms. The main body of the instrument adopted 201 stainless steel material and an electrostatic powder spraying process; the control system was based on the Android 11 platform and equipped with a 10.1-inch touch screen, supporting Wi-Fi/4G/Ethernet multi-mode data transmission, and integrated temperature, humidity and voltage sensors to monitor equipment status in real time.

Performance evaluation showed that the instrument achieved full-process unattended operation from spore capture, imaging, and upload to recognition. Users could perform remote control (parameter setting, equipment restart, remote focusing) and real-time data monitoring through a dedicated app, WeChat mini-program or Web terminal, and receive WeChat early warning information, realizing remote intelligent operation and maintenance. The instrument operated stably in a wide temperature range of -20°C to 70°C and a relative humidity of up to 95%, with power consumption lower than 20 W, and had power-off memory and automatic calibration functions, meeting the reliability requirements for long-term field deployment. Practical applications confirmed that the instrument significantly improved spore monitoring efficiency, and its cloud data platform provided effective technical support for the epidemic prediction of wheat stem rust.

Figure 8. Wheat straw rust analyzer

4. Conclusion

In summary, this study successfully developed a spore capture and analyzer integrating microfluidic capture, automatic imaging, and intelligent recognition functions. The chip structure was optimized via numerical simulation, and experiments verified that its actual enrichment efficiency for Pgt urediniospores reached 86.67%; the spore recognition model constructed based on YOLOv8 had high accuracy (mAP@50 = 96.7%) and strong generalization ability; the whole machine realized full-process unattended operation under wide temperature and humidity conditions, and remote operation and maintenance and data management through the cloud platform. This instrument provides a reliable technical means for early warning and epidemic prediction of wheat stem rust and improves the automation and intelligence level of monitoring airborne wheat stem rust spores.

Funding

This work was supported by the National Key Research and Development Program of China (Grant No. 2023YFC2604903) and the Tuoxin Team Cultivation Project of Henan University of Technology (Grant No. 2024TXTD13).

Disclosure statement

The authors declare no conflict of interest.

References

[1] Figueroa M, Upadhyaya NM, Sperschneider J, et al., 2016, Changing the Game: Using Integrative Genomics to Probe Virulence Mechanisms of the Stem Rust Pathogen *Puccinia graminis f. sp. tritici*. Frontiers in Plant Science, 2016(7): 205.

[2] Zhao J, Kang Z, 2023, Fighting Wheat Rusts in China: A Look Back and into the Future. Phytopathology Research, 2023(5): 6.

[3] Sun ZY, Wei YF, Sun HY, et al., 2025, Evaluation of Stem Rust Resistance and Molecular Detection of Sr31 in 36 Wheat Varieties (lines) from Henan Province. Plant Protection, 2025(51): 360–365.

[4] Cao Y, Si B, Zhu G, et al., 2019, Race and Virulence of Asexual and Sexual Populations of *Puccinia graminis f. sp. tritici* in China from 2009 to 2015. European Journal of Plant Pathology, 2019(153): 545–555.

[5] Figlan S, Roux CL, Terefe T, et al., 2014, Wheat Stem Rust in South Africa: Current Status and Future Research Directions. African Journal of Biotechnology, 2014(13): 4188–4199.

[6] Gao F, Wu X, Sun H, et al., 2024, Identification of Stem Rust Resistance Genes in Triticum Wheat Cultivars and Evaluation of their Resistance to *Puccinia graminis f. sp. tritici*. Agriculture, 2024(14): 198.

[7] Sharma RK, Singh PK, Vinod, et al., 2013, Protecting South Asian Wheat Production from Stem Rust (Ug99) Epidemic. Journal of Phytopathology, 2013(161): 299–307.

[8] Mushtaq S, Afzal A, Ibrahim A, et al., 2025, Genetic Frontiers against the Ug99 Threat. Planta Animalia, 4(1): 39–51.

[9] Szabo LJ, Olivera PD, Wanyera R, et al., 2022, Development of a Diagnostic Assay for Differentiation between Genetic Groups in Clades I, II, III, and IV of *Puccinia graminis f. sp. tritici*. Plant Disease, 106(8): 2211–2220.

[10] Zhao X, Zhai L, Chen J, et al., 2024, Recent Advances in Microfluidics for the Early Detection of Plant Diseases in Vegetables, Fruits, and Grains Caused by Bacteria, Fungi, and Viruses. Journal of Agricultural and Food Chemistry, 72(28): 15401–15415.

[11] Zhang X, Bian F, Wang Y, et al., 2022, A Method for Capture and Detection of Crop Airborne Disease Spores Based on Microfluidic Chips and Micro Raman Spectroscopy. Foods, 11(21): 3462.

[12] Wang Y, Zhang X, Yang N, et al., 2021, Separation-enrichment Method for Airborne Disease Spores Based on Microfluidic Chip. International Journal of Agricultural and Biological Engineering, 14(5): 199–205.

[13] Shakeri A, Khan S, Didar TF, 2021, Conventional and Emerging Strategies for the Fabrication and Functionalization of PDMS-based Microfluidic Devices. Lab Chip, 2021(21): 3053–3075.

[14] Hassan HM, Amir A, El-Ghany ANM, et al., 2025, Aspergillus Detection Based on Deep Learning Model Using YOLOv8 with a Small Custom Dataset. Egyptian Journal of Botany, 65(2): 211–226.

[15] Sun HY, 2024, Mechanism of TaERF60-mediated Wheat Stem Rust Resistance and Resistance Source Mining, thesis, Shenyang Agricultural University.